Applied Catalysis B: Environmental 107 (2011) 34–41

Contents lists available at ScienceDirect

Applied Catalysis B: Environmental

journal homepage: www.elsevier.com/locate/apcatb

Quantitative room-temperature mineralization of airborne formaldehyde using manganese oxide catalysts

Meera A. Sidheswaran[a], Hugo Destaillats[a,b,*], Douglas P. Sullivan[a], Joern Larsen[c], William J. Fisk[a]

[a] Lawrence Berkeley National Laboratory, Environmental Energy Technologies Division, Berkeley, CA, USA
[b] Arizona State University, School of Sustainable Engineering and the Built Environment, Tempe, AZ, USA
[c] Lawrence Berkeley National Laboratory, Earth Sciences Division, Berkeley, CA, USA

ARTICLE INFO

Article history:
Received 6 April 2011
Received in revised form 3 June 2011
Accepted 20 June 2011
Available online 30 June 2011

Keywords:
Manganese oxide catalysts
Room-temperature oxidation
Mineralization
Indoor air
Formaldehyde

ABSTRACT

Manganese oxide-based catalysts have been synthesized and tested for the abatement of formaldehyde, an ubiquitous indoor pollutant which is not effectively eliminated by most air cleaning technologies. Catalysts were prepared by co-precipitation of $MnSO_4$ and $NaMnO_4$ followed by curing at 100, 200 and 400 °C. Characterization was performed using X-ray diffractometry (XRD), porosimetry, scanning electron microscopy (SEM), and inductively coupled plasma-mass spectrometry (ICP-MS). Diffractograms of samples treated at 100 and 200 °C matched those of nsutite and cryptomelane/manjiroite structures, with high BET surface area (up to 149 $m^2\,g^{-1}$) and small particle size (<50 nm), while curing at 400 °C yielded pyrolusite with lower effective surface area. Room temperature catalytic oxidation of airborne formaldehyde was studied by supporting the catalyst on a particulate filter media placed in a flow system, under stable upstream formaldehyde concentrations between 30 and 200 ppb. Two different face velocities (v = 0.2 and 50 cm s^{-1}) were studied to evaluate the oxidation efficiency under different flow regimes using formaldehyde-enriched laboratory air at 25–30% relative humidity. Results showed consistent single-pass formaldehyde oxidation efficiency greater than 80% for the synthesized catalysts, which remained active over at least 35 days of continuous operation at v = 0.2 cm s^{-1} and were able to process up to 400 m^3 of air at v = 50 cm s^{-1} without appreciable deactivation. Operation under high relative humidity (>90% RH) produced only a small reversible reduction in formaldehyde removal. Most significantly, 100% mineralization yields were verified by quantifying CO_2 formation downstream of the catalyst for upstream formaldehyde concentrations as high as 6 ppm and a face velocity of v = 13 cm s^{-1}. In contrast, a filter loaded with commercially available MnO_2 did not remove appreciable amounts of formaldehyde at v = 50 cm s^{-1}, and yielded <20% initial removal when operated at a very low face velocity (v = 0.03 cm s^{-1}). Due to the relatively low costs of synthesis and deployment of these catalysts, this technology is promising for maintaining low indoor formaldehyde levels, enabling energy-saving reductions of building ventilation rates.

1. Introduction

Manganese dioxide (MnO_2) is a relatively abundant and inexpensive material. Manganese oxide-based nanoparticles have been used for water purification for a long time [1]. The redox properties of manganese oxide minerals make them useful catalysts in industrial processes. Naturally occurring manganese oxides have a MnO_6 octahedral structure that assembles into a large variety of structural arrangement, yielding minerals with high surface area. Also, multiple oxidation states of Mn atoms in a single mineral facilitate catalyzing oxidative processes [2]. A great deal of attention has been placed recently on the synthesis of novel MnO_2-based catalysts for the removal of formaldehyde and other volatile organic compounds (VOCs) at room or low temperatures (<100 °C) [3,4]. Airborne formaldehyde removal efficiency were estimated for coated honeycomb substrates with various dimensions, indicating that up to 20% formaldehyde removal efficiency could be obtained with very low pressure drops (about 2–3 Pa) operating at face velocities typical of air filtering systems (1–3 m s^{-1}) [4]. In addition to active air cleaning applications, there is some additional evidence of Mn-based catalyst efficacy in passive applications. In a residential setting, deployed manganese oxide within wallboard was reported to reduce 50–80% of indoor formaldehyde levels throughout a 7-month long study period [5].

Other metal oxides such as Co_3O_4 and Co_3O_4–CeO_2 mixtures, have also been shown to remove CO and formaldehyde at

* Corresponding author at: Lawrence Berkeley National Laboratory, Environmental Energy Technologies Division, Berkeley, California, USA. Tel.: +1 510 486 5897; fax: +1 510 486 7303.
E-mail address: HDestaillats@lbl.gov (H. Destaillats).

0926-3373/$ – see front matter © 2011 Elsevier B.V. All rights reserved.
doi:10.1016/j.apcatb.2011.06.032

room temperature [6,7]. Doping of MnO_2 with transition metals and synthesis of mixed oxides containing Mn showed improved formaldehyde removal efficiencies. For example, MnO_x–CeO_2 catalysts had better performance than MnO_2 synthesized by the same method [8,9]. Also, other authors showed good performance of manganese oxides doped with vanadium [10] and tin [11]. Several commercial catalysts (e.g., CARULITE®) contain hopcalite, a mixture of MnO_2 and CuO, often combined with other metal oxides. While those catalysts provide efficient CO and ozone removal at room temperature, they often require higher temperatures for reactions with organic pollutants, and are sensitive to moisture [6]. In particular, hopcalite was shown to be effective only at temperatures higher than 250 °C for the oxidation of volatile organic compounds produced as byproducts of combustion (e.g., acetone) [12] and for the oxidation of propane [13].

Several manganese oxide nano and meso structures (e.g., pyrolusite, cryptomelane) have been shown to have very high catalytic activity in the oxidation of formaldehyde at relatively low temperatures (100 °C). Such enhanced catalytic properties were explained by their porosity, tunnel structures, degree of crystallinity, reducibility and average oxidation state of the manganese atoms [14,15]. Nano-structured mixed valence oxides (such as Mn_3O_4) were shown to effectively catalyze the oxidation of formaldehyde at room temperature [16]. In most of the cases mentioned here, low temperature oxidation of formaldehyde likely takes place via a Mars–van Krevelen (MvK) mechanism, as is usually described for high temperature catalysis, in which lattice oxygen atoms from the catalyst participate in the initial step of the reaction, and are subsequently replenished by reduction of atmospheric O_2 [17,18]:

$$MnO_{x-1}\text{–}O(s) + CH_2O(ads) \rightarrow MnO_{x-1}(s) + 2H(ads) + CO_2(g) \quad (1)$$

$$MnO_{x-1}(s) + 2H(ads) + O_2(g) \rightarrow MnO_{x-1}\text{–}O(s) + H_2O(g) \quad (2)$$

In this mechanism, catalyst efficiency is associated with the number of active surface sites with Mn atoms susceptible to be cyclically reduced and re-oxidized as shown in Eqs. (1) and (2). Formic acid can be formed as a side product of incomplete oxidation, and may be found in the gas phase or adsorbed to the catalyst.

Formaldehyde is a ubiquitous indoor air pollutant of concern, listed as a human carcinogen by the World Health Organization and as a probable human carcinogen by the US Environmental Protection Agency [19,20]. Its indoor sources include composite and laminated wood-based building products [21], operation of office equipment [22], and ozone-driven indoor chemistry [23,24]. Indoor formaldehyde levels measured in surveys of US commercial and residential buildings were as high as 42 ppb and 37 ppb, respectively [25,26], often exceeding recommended exposure limits [27]. In some buildings, formaldehyde removal is one of the limiting factor determining minimum building ventilation rates and air cleaning requirements. Hence, cost-effective and practical formaldehyde abatement technologies may enable significant ventilation energy savings.

In this study, we synthesized novel MnO_x catalysts (with $1 \ll x \leq 2$) and used them to coat the surface of ventilation filtering media with a moderately low pressure drop. We evaluated experimentally the efficiency of formaldehyde elimination under various flow regimes and pollutant concentrations. We also determined the extent of mineralization and explored the formation of intermediate gas-phase byproducts. Our results illustrate the potential of this approach as an effective indoor pollution mitigation technology. For example, low cost particle filters coated with these catalysts may be installed in ventilation systems over 6-month periods, or for up to 12 months if protected by a pre-filter.

2. Experimental methods

2.1. Preparation of manganese oxide catalysts

Sodium permanganate (≥97%, with traces of potassium impurities) and manganese sulfate monohydrate (≥98%) were obtained from Sigma–Aldrich and used without further purification. Manganese dioxide (>98%) was also obtained from Sigma–Aldrich to use as a reference in formaldehyde removal tests.

Previous studies have shown that manganese oxide synthesized via the co-precipitation route had desirable oxidative catalytic properties [28]. Manganese sulfate ($MnSO_4$) and sodium permanganate ($NaMnO_4$) were dissolved in deionized water. The sodium permanganate solution was added slowly drop wise to the manganese sulfate aqueous solution, with constant stirring such that the molar ratio of the resulting solution was maintained at a ratio 2:3 $NaMnO_4$:$MnSO_4$, leading to precipitation of an oxide. The resulting suspension was kept at room temperature for 24 h, filtered, and the precipitate was washed with deionized water. Three different aliquots of the precipitate transferred to Petri dishes were heated in air for 12 h at 100, 200 and 400 °C, respectively, to prepare three different catalysts.

2.2. Catalyst characterization techniques

2.2.1. BET surface area and pore size distribution

The Brunner, Emmet and Teller (BET) surface area was determined using a Porosimeter analyzer (Micromeritics 3000). Nitrogen was used as the sorption gas to study the N_2-BET isotherm and obtain the surface area. Pore size distribution was determined using the BJH method. About 1 g of each sample was previously degassed for a period of 12 h under a stream of nitrogen at 100 °C.

2.2.2. X-ray diffractometry

The material was ground under hexane, and a few drops of the slurry were applied onto a silicon zero background plate (ZBP) placed on a warm hotplate. When dry, the ZBP was placed in a holder and examined using a Panalytical X'Pert diffractometer with Cu anode. Raw X-ray diffraction data were merged (12, 2 h scans), an empirical background was removed, the K alpha 2 contribution was stripped, and the scans were smoothed using a Fourier filter. Peaks were selected using the peak picking utility, and phases were determined using a library search by matching utility with all manganese files in the database. Crystallite size was obtained using the Scherrer equation.

2.2.3. SEM imaging analysis

SEM imaging was performed using a Hitachi SE4000 scanning electron microscope. Samples were mounted on a specimen support and sputter coated with gold nano-particles before analysis.

2.2.4. ICP-MS analysis

The elemental composition of macro constituents and traces in manganese oxide samples was analyzed using a Perkin Elmer DRCII inductively coupled plasma-mass spectrometer (ICP-MS). To measure the concentrations of trace impurities such as Mg, K and Fe, the instrument was used in DRC (dynamic reaction cell) mode using ammonia as reaction gas to remove interferences. Other elements were analyzed in standard mode. Gallium was used as an internal standard.

2.3. Evaluation of formaldehyde elimination

2.3.1. Preparation of supported catalysts

Formaldehyde removal was studied using a continuous flow system. The catalyst support used in this study was a 1-in. thick

polyester heating ventilation and air conditioning (HVAC) particle filter with a thin tackifier coating (AAF International, KY). The MnO_x sample conditioned at 100 °C (LBNL-100) was chosen for these tests due to its higher BET surface area. The catalyst was ground into a fine powder and transferred into a Petri dish. A 47 mm-diameter HVAC filter media specimen was mounted on an open faced filter holder with the loading side visible. The filter holder was fitted to the Petri dish holding the manganese oxide, and connected to laboratory vacuum for 10 min, allowing for elutriation of manganese oxide particles from the Petri dish to the filter surface. The mass of LBNL-100 manganese oxide loaded on the filter surface (110 mg) was obtained by weighing the filter before and after loading. The filter was then removed from the open faced filter holder and transferred into a 47-mm custom made alumina filter holder with 10 cm^2 of open area. The procedure was repeated with a similar filter for commercially obtained MnO_2, used to compare the performance efficiency between the laboratory-prepared catalyst and a reference material. The mass of commercial MnO_2 deposited on the filter following the same procedure was 320 mg. A test using Carulite 110-A, a commercial catalyst containing MnO_2, was also carried out under identical conditions, with a filter containing 265 mg of catalyst.

2.3.2. Experimental setup

Formaldehyde-enriched indoor air was generated using two different experimental setups. In one case, we used as a formaldehyde source seven 4 × 4 sq. in. highly emitting specimens of cabinetry obtained in a recent study [29]. These stable diffusive sources were placed inside a 200-L bench chamber ventilated at an air exchange rate of less than 0.15 h^{-1} with laboratory air at 25–30% relative humidity, generating formaldehyde concentrations in the range 150–200 ppb. The other setup consisted on a 20-m^3 room-sized chamber ventilated at an air exchange rate of 1 h^{-1} at 25–30% relative humidity, in which lower levels of formaldehyde (30–40 ppb) were achieved by continuously infusing an aqueous solution of the target compound using a syringe pump. Two experiments at different face velocities were conducted using each of the experimental setups, to evaluate the efficiency of the catalyst at high and low air flows. Air from each of the chambers was pulled through the filter holder containing the supported manganese oxide catalyst at the rate of 0.1 L min^{-1} (bench chamber) and 30 L min^{-1} (room-sized chamber). These corresponded to a face velocity of 0.17 cm s^{-1} and 52.4 cm s^{-1}, respectively (which are rounded here to 0.2 and 50 cm s^{-1}, respectively). The latter is within the range of air velocities achieved at filtration media used in building HVAC systems, typically between ~0.3 and 1 m s^{-1}. Formaldehyde samples were collected simultaneously upstream and downstream of the filter holder in all cases.

2.3.3. Sampling and analytical methods

Integrated volatile carbonyl samples were collected upstream and downstream of the catalyst using dinitrophenyl hydrazine (DNPH)-coated silica samplers (Waters) at a rate of 20 cm^3 min^{-1} for the commercial catalyst or 100 cm^3 min^{-1} for LBNL-100 using peristaltic pumps (this amounted to the total flow through the supported catalyst for experiments carried out at v = 0.2 cm s^{-1}). Ambient ozone was removed with potassium iodide scrubbers preceding each DNPH sampler (Waters Sep-pak Ozone scrubber). The concentration value reported in each case corresponds to a time-integrated average over the sampled period, and is reported at the center of each sampling period. The flow corresponding to each sample was measured using a primary air flow calibrator (Gilibrator®) with a precision greater than 2%.

DNPH cartridges were extracted with 2-mL aliquots of acetonitrile, and the extracts were analyzed by HPLC with UV detection at λ_{max} = 360 nm (Agilent 1200). A calibration curve for quantification was carried out using authentic standards of the formaldehyde-DNPH hydrazone.

2.4. Evaluation of the extent of mineralization

Carbon dioxide levels produced as a final byproduct of formaldehyde mineralization were estimated in separate tests using a mid-IR online analyzer (Picarro iCO_2, CBDS 07). Ultrahigh purity nitrogen and oxygen (99.999% pure) (Alliance Gas) with minimal CO_2 background levels (<1 ppb) were used for this evaluation. A gas stream was connected to a formaldehyde source consisting of 20 mL of a 37% aqueous formaldehyde solution in a 100 mL beaker, which was placed inside a 4-L stainless steel flow cell. The net flow of gas mixture through the flow cell was maintained at 8 L min^{-1}, corresponding to a face velocity of 0.13 m s^{-1}. The nitrogen-to-oxygen ratio was ~7:3. Upstream and downstream gas samples were collected in two 5-L Mylar bags for off-line CO_2 analysis. Formaldehyde present in upstream and downstream samples was stripped using DNPH-coated silica cartridges (Waters Sep-pak) to avoid spectral interference with the iCO_2 analyzer. These cartridges were subsequently extracted with acetonitrile for aldehyde analysis as described above (Section 2.3.3). In order to analyze the possibility of partial oxidation by-products, tests were also conducted to identify the formation of formic acid. For that purpose, upstream and downstream samples were collected through bubbling in a 0.01 N sodium hydroxide solution placed in glass impingers, subsequently analyzed by Ion Chromatography (Dionex ICS 2000). Standards were prepared using 1 g L^{-1} sodium formate solution (Sigma–Aldrich, Formate standard for IC) to identify and quantify the formate ion.

3. Results and discussion

3.1. Catalyst characterization

3.1.1. BET surface area and pore size distribution analysis

BET surface area measurements obtained for the different materials tested in this study are listed in Table 1.

The BET surface area of the manganese oxide samples synthesized in our lab decreased with increased curing temperature. For the commercial manganese dioxide sample, the BET area was significantly lower (by factors of 23–37) than the samples prepared in the lab. Fig. 1 illustrates the BJH pore size distribution obtained in each case. Most of the available surface area in the materials synthesized in our laboratory corresponds to pore sizes smaller than 10 nm, in contrast to the commercial MnO_2 sample. The temperature during catalyst synthesis also has an effect on pore structure as shown in Fig. 1. With increase in temperature the pore size distribution shifted slightly towards higher size, and the pore volume decreased, consistent with the lower BET surface area (Table 1).

3.1.2. X-ray diffraction analysis

Results of X-ray diffractometry for the different preparations of manganese oxide are shown in Fig. 2. Table 2 shows the composition and crystallite size of each sample. For LBNL-100 and LBNL-200, the X-ray diffraction spectra show combinations of intense and weak reflections characteristic of the nsutite and cryptomelane/manjiroite phases; the sample treated at 400 °C was

Table 1
BET surface area of different manganese oxides.

Sample	Curing temperature (°C)	BET surface area (m^2 g^{-1})
LBNL-100	100	149
LBNL-200	200	103
LBNL-400	400	93
Commercial MnO_2	–	4

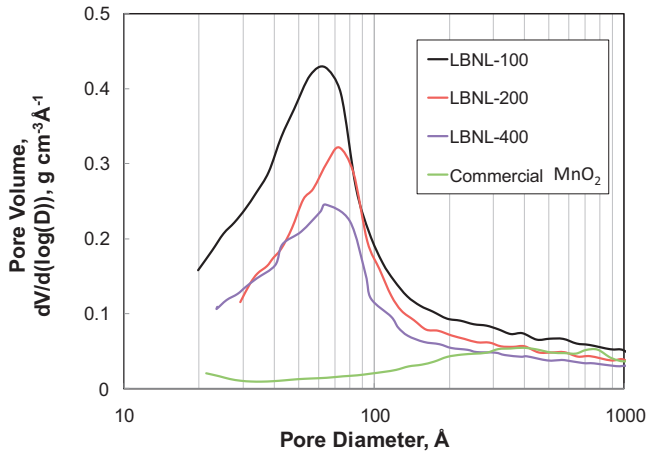

Fig. 1. BJH pore size distribution of synthesized samples and commercial MnO_2.

consistent primarily with pyrolusite signatures [14,30]. The crystallite sizes for the LBNL samples were observed to be in the range of 5.9–10 nm. Changes in the X-ray diffractograms show that phase change occurs, leading to larger crystallite size as curing temperature increased. The commercially available manganese oxide is reported as pyrolusite.

X-ray diffraction spectra were also obtained from manganese oxide samples after having catalyzed the oxidation of formaldehyde over several weeks. The X-ray spectra of manganese oxide after multiple catalytic cycles showed no visible phase change, and no permanent change of the oxidation state of surface species.

3.1.3. SEM surface analysis

Fig. 3(a)–(c) shows the scanning electron microscopy (SEM) images of manganese oxide samples LBNL-100, LBNL-200 and LBNL-400, respectively. Fig. 3(d) shows the SEM image of commercially available MnO_2.

The manganese oxide samples synthesized in the lab were highly porous and had monodisperse nanospherical particles with diameter smaller than 50 nm. This is consistent with the small crystallite size determined by XRD. The commercially available manganese oxide had particles with well defined crystal shape and size greater than 2 μm. It can be seen from SEM images of the laboratory synthesized manganese oxide that each nanospherical particle consisted of platelets that were aligned perpendicular to the spherical surface. This structural formulation is due to the hydrothermal precipitation method of synthesis of these materials, and suggests the presence of voids that can incorporate water in interstitial spaces [31,32].

3.1.4. Determination of empirical formulae

The results from ICP-MS analysis are shown in Table 3, and are in accordance with those from X-ray diffraction studies. We identified manganese as the main constituent, together with minor

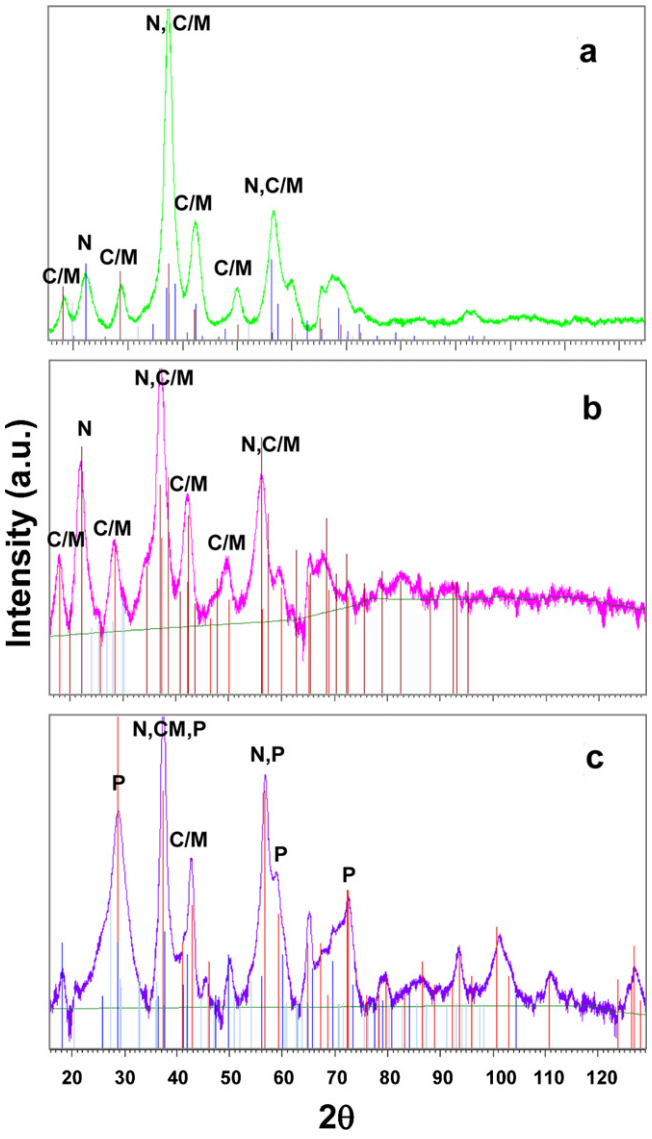

Fig. 2. X-ray diffraction spectrum of MnO_x treated at (a) 100 °C; (b) 200 °C; and (c) 400 °C. N: nsutite; C/M: cryptomelane/manjiroite; and P: pyrolusite.

constituents such as sodium and potassium, as well as other trace impurities (e.g., iron). Based on the results obtained from X-ray diffraction, we quantitatively estimated the mineral allotropic form and the oxidation state of manganese in the LBNL samples using the data from ICP-MS analysis. The sodium and potassium mass obtained from the analysis was used to estimate the amount of cryptomelane and manjiroite present in each of the LBNL samples. Manganese present in cryptomelane and manjiroite was estimated from the corresponding empirical formula, and the remainder of

Table 2
Composition of manganese oxide prepared in the laboratory.

Material	Compound name	Chemical formula	Crystallite size (nm)
LBNL-100	Nsutite Cryptomelane/manjiroite	$Mn_{1-x}^{4+}Mn_x^{2+}O_{2-2x}(OH)_{2x}$[a] $(Na,K)_x(Mn^{4+}Mn^{3+})_8O_{16}$[b]	4.0–6.4
LBNL-200	Nsutite Cryptomelane/manjiroite	$Mn_{1-x}^{4+}Mn_x^{2+}O_{2-2x}(OH)_{2x}$[a] $(Na,K)_x(Mn^{4+}Mn^{3+})_8O_{16}$[b]	6.6–10
LBNL-400	Pyrolusite Cryptomelane/manjiroite	MnO_2 $(Na,K)_x(Mn^{4+}Mn^{3+})_8O_{16}$[b]	8.4–10

[a] Where $x = 0.06–0.07$, corresponding to a mixture of 12% MnO/85% MnO_2.
[b] Ref. [2].

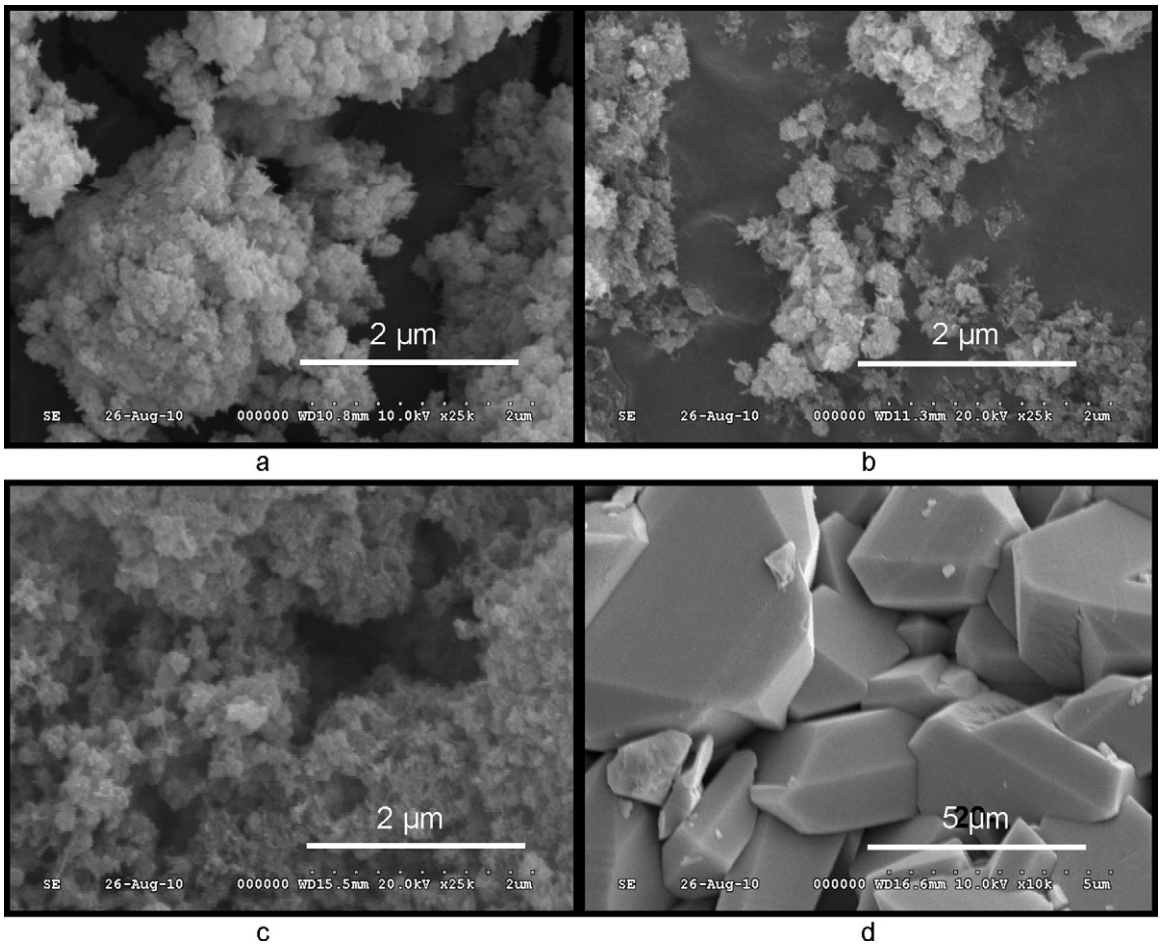

Fig. 3. SEM images of manganese oxide particles synthesized and treated at (a) 100 °C; (b) 200 °C; (c) 400 °C; and (d) commercially available MnO_2.

the manganese mass was assigned to the nsutite phase. The difference between the total mass estimated using the stoichiometric formulas and the sample mass is attributed to water incorporated into interstitial voids of manganese oxide, and reported in Table 3. To verify this assumption, we heated a known mass of LBNL-100 after synthesis at 80 °C for a period of 12 h, observing a ~13% decrease in sample mass, consistent with the mass of water indicated in Table 3. Previous studies on thermal evolution of water from manganese oxides have shown that moisture content decreased with increasing curing temperature, and was reduced drastically at 500 °C [33]. In order to maintain electroneutrality in the presence of cations such as Na or K at the grain boundary or in the tunnel structures, Mn^{4+} is partially substituted by Mn^{3+}. The multiple oxidation states present in samples LBNL-100 and LBNL-200, as well as the presence of large tunnels where water uptake is facilitated by cations [2,34] are likely the reason of the high catalytic activity of these minerals. The tunnel structure of pyrolusite (the predominant form in samples treated at 400 °C) is smaller, and hence cannot hold as much water as samples LBNL-100 and LBNL-200.

Table 3
Elemental analysis of MnO_x samples using ICP-MS.

Sample	MnO_x:H_2O ratio (mass%)	Element	Mass fraction present in the sample	MnO_x phase and empirical formula
LBNL-100	85:15	Mn Na K Fe	63.1 0.35 0.29 0.03	84% nsutite, 2% cryptomelane, 13% manjiroite
LBNL-200	84:16	Mn Na K Fe	63.0 0.37 0.26 0.04	84% nsutite, 2% cryptomelane, 13% manjiroite
LBNL-400	91:9	Mn Na K Fe	63.1 0.04 0.03 0.04	99% pyrolusite, traces of manjiroite and cryptomelane

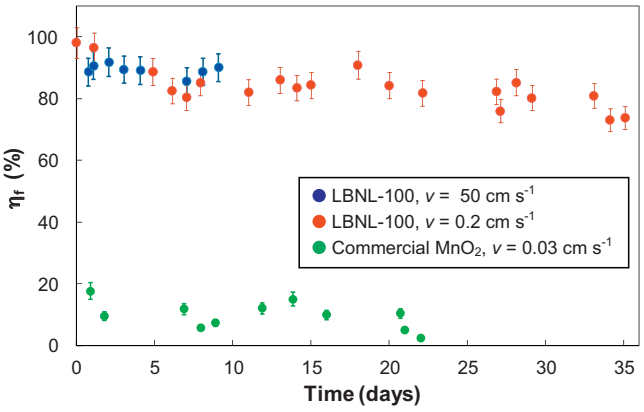

Fig. 4. Formaldehyde removal η_f vs. time.

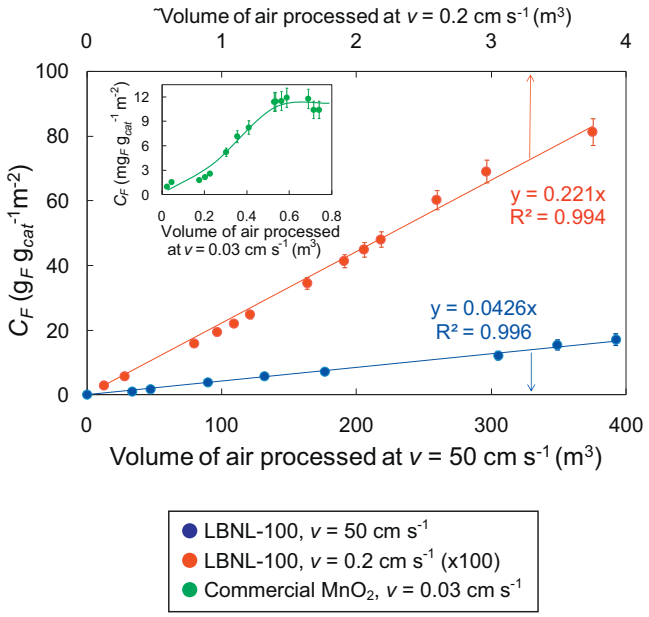

Fig. 5. Cumulative formaldehyde mass reacted per unit filter face area and unit mass of catalyst (C_F) as a function of the volume of air processed by the supported catalyst. Insert plot corresponds to C_F of commercial MnO_2 (note different C_F units for the insert, expressed in $mg_F\ g_{cat}^{-1}\ m^{-2}$).

3.2. Formaldehyde elimination

Formaldehyde removal efficiency (η_F) was calculated with Eq. (3) where $[F]_{up}$ and $[F]_{dn}$ are the upstream and downstream formaldehyde concentration, respectively (both expressed in $\mu g\,m^{-3}$),

$$\eta_F = \left(\frac{[F]_{up} - [F]_{dn}}{[F]_{up}}\right) \times 100 \quad (3)$$

Fig. 4 shows the efficiency of the LBNL-100 manganese oxide catalyst to remove formaldehyde at two different face velocities, together with data corresponding to commercially available manganese dioxide. For the low face velocity conditions ($v = 0.2\,cm\,s^{-1}$), the formaldehyde levels upstream were maintained at 150–200 ppb, while for high face velocity ($v = 50\,cm\,s^{-1}$) the formaldehyde concentration was maintained at 30–45 ppb, which is ~5 times lower than in experiments carried out at $v = 0.2\,cm\,s^{-1}$, and closer to levels typically found in buildings. The filter containing the laboratory-synthesized manganese oxide LBNL-100 performed significantly better than commercial MnO_2, despite having only ~1/3 of the catalyst mass loading. High formaldehyde removal results (>80%) obtained for LBNL-100 at $v = 50\,cm\,s^{-1}$ were similar to those observed for the lower face velocity. In order to test a worst-case scenario condition, a separate short test (not shown in Fig. 4) was carried out for a period of 12 h with a high formaldehyde concentration of 150 ppb and the high face velocity of $v = 50\,cm\,s^{-1}$. Under these extreme conditions, the removal efficiency η_F was still higher than 60%. By contrast, a filter loaded with commercial MnO_2 was only able to remove less than 5–10% of formaldehyde (within the experimental error of the determination) when operated over a 4-day period at $v = 50\,cm\,s^{-1}$. Even at a very low face velocity ($v = 0.03\,cm\,s^{-1}$, data shown in Fig. 4), the efficiency of the commercial MnO_2 was poor, not exceeding 20% removal initially, and decreased over time due to inactivation. The MnO_2-containing commercial catalyst Carulite 110-A showed a 3.5% removal efficiency after 25 h of operation under identical conditions (not shown in Fig. 4).

Fig. 5 shows the cumulative mass of formaldehyde reacted per unit filter face area and unit mass of catalyst (C_F) in experiments carried out with the filter loaded with LBNL-100 operating at the two different face velocities, as a function of the volume of air processed. The choice of this independent variable better illustrates the capacity of the catalyst for effective formaldehyde elimination up to a total air volume of 400 m^3, showing linear behavior spanning a range of two orders of magnitude for this variable. The cumulative mass of formaldehyde per unit area was defined as

$$C_F = \frac{1}{W_C S}\int_0^t f[F]_{up} \times \frac{\eta_F}{100} \times dt \quad (4)$$

where W_C is the mass of the catalyst (in g), S is the filter face area (in m^2) and f is the air flow (in $m^3\,min^{-1}$). The cumulative formaldehyde mass removed increased linearly under both flow regimes, because the removal efficiency of the LBNL-100 catalyst was relatively constant during the studied periods. Since the volume of air processed at $v = 50\,cm\,s^{-1}$ was ~100 times higher than the volume of air processed at $v = 0.2\,cm\,s^{-1}$, the C_F values increased proportionally. The difference in slopes observed in Fig. 5 can be attributed to the differences in upstream formaldehyde concentrations between both experiments, with ~5 times higher $[F]_{up}$ for the experiment carried out at $v = 0.2\,cm\,s^{-1}$.

Fig. 5 illustrates also the cumulative mass of formaldehyde C_F removed by the commercial MnO_2 operating at a low face velocity (shown in insert). The amount of formaldehyde removed using MnO_2 over a 23-day period at $v = 0.03\,cm\,s^{-1}$ was only $10\,mg\,m^{-2}\,g^{-1}$ catalyst, equivalent to ~10% of the total formaldehyde removed with the LBNL-100 catalyst for the same volume of air processed. This difference in the initial removal capacity of each catalyst can be attributed to the higher available surface area of LBNL-100. Considering the amount of catalyst deposited in each filter and their respective BET surface area, the effective area ratio was one order of magnitude higher for LBNL-100. For the commercial MnO_2, saturation and loss of catalytic capacity was observed after a relatively low volume of air processed (~0.6 m^3), in contrast with results obtained with LBNL-100 showing no significant loss of performance up to 400 m^3 of air processed. Hence, intrinsic redox properties of LBNL-100 likely played a significant role in its much longer lifetime.

Table 4
Formaldehyde and carbon dioxide upstream and downstream concentrations.

Experiment number	Compound	Concentration (ppm)		
		Upstream	Downstream	*Difference*
1	Formaldehyde	6.06 ± 0.16	1.97 ± 0.05	*−4.09 ± 0.21*
	Carbon dioxide	0.04 ± 0.19	4.11 ± 0.18	*4.07 ± 0.37*
2	Formaldehyde	2.84 ± 0.09	0.88 ± 0.03	*−1.96 ± 0.12*
	Carbon dioxide	0.62 ± 0.30	2.54 ± 0.07	*1.92 ± 0.37*

3.3. Mineralization

The oxidation of formaldehyde catalyzed by manganese oxides following the MvK mechanism (Eqs. (1) and (2)) leads ultimately to mineralization, i.e., to the formation of carbon dioxide and water. The concentration of CO_2 released from the oxidation of formaldehyde was measured to evaluate the extent of mineralization under the current experimental conditions. The upstream and downstream formaldehyde and carbon dioxide concentrations were recorded in two separate experiments, and are listed in Table 4. These tests were performed at higher formaldehyde concentrations than the experiments reported above in Section 3.2 (by a factor of between 15 and 200 higher) due to the relatively low sensitivity of the iCO_2 analyzer. Within the experimental error, the extent of mineralization was 100% in both experiments. These results suggest that formaldehyde undergoes complete conversion into CO_2 and H_2O, in good agreement with the proposed MvK mechanism, even at concentrations that are much higher than those typically found in buildings. Therefore, it can be expected that for typical building levels of formaldehyde (in the tens of ppb), complete mineralization will also be achieved. Formic acid, a potential intermediate byproduct, was not detected in samples collected downstream of the catalyst, lending further support to the above observation of a complete formaldehyde mineralization.

3.4. Effect of the relative humidity

The filter loaded with LBNL-100 was tested using an airstream saturated with water (RH > 90%) for a period of 100 h at a face velocity of 50 cm s^{-1}, during which the formaldehyde conversion was ~80%. This is slightly lower than the formaldehyde conversion at 25–30% RH reported above (Section 3.2) where formaldehyde conversions were as high as 85–90%. When the humidity in the system was reduced back to 25% RH, the percent removal of formaldehyde increased to 85% showing the ability of the catalyst to regenerate at lower humidity. The slight decrease in formaldehyde removal efficiency at high ambient humidity conditions can be attributed to the competitive adsorption of water on the surface of the catalyst. However, formaldehyde is soluble in water and hence can be trapped reversibly in the sorbed aqueous layer, leading to consistent removal of formaldehyde with minimal effect on catalyst performance due to changes in relative humidity.

4. Practical implications for air cleaning and building energy efficiency

Building mass balance modeling indicate that, assuming typical ratios of outdoor air ventilation flow to total supply air flow in commercial building HVAC systems, a ~20% formaldehyde removal efficiency in the supply airstream would be adequate to counteract the expected indoor formaldehyde increases associated with a 50% reduction in minimum outdoor air supply. Our results suggest that formaldehyde removal efficiencies can substantially exceed 20% if the HVAC system contains filters supporting the manganese oxide catalyst synthesized in our laboratory. In some buildings, formaldehyde-control alone may enable energy-saving reductions in ventilation rates, because the risks of formaldehyde dominate relative to the risks of other indoor-generated pollutants with concentrations controlled by ventilation. In other buildings, if the catalyst-loaded filters can be supplemented by air cleaning systems [35] or by source control measures for other pollutants, improvements in indoor air quality and simultaneous significant ventilation energy savings may be achieved.

This study has only considered initial catalyst performance, and has not focused on identifying factors that may cause poisoning of the catalyst. Previous studies carried out at high temperatures have shown that manganese oxide catalyst inactivation can occur due to the deposition of elemental carbon and sulfur resulting from the oxidation reaction of organics on the surface [36]. Similarly, dust particles deposited on the filter may partially block the catalyst surface and increase its moisture content, becoming a source of secondary pollutants and affecting catalyst performance [37]. The reduction of the surface Mn(III) ions to Mn(II) leading to oxygen depletion coupled with loss of some surface species such as sodium can also decrease catalytic activity [38]. Long-term studies are being currently conducted to evaluate the lifetime of the catalyst. Further, the effect of the presence of other VOCs is also being evaluated. Preliminary evidence suggests that the catalyst is not easily deactivated, as shown in the experiments described in this article, carried out with cabinetry specimens as a source of formaldehyde. The air used in this study was drawn directly from the laboratory, and contains a broad range of VOCs, in addition to those emitted by the cabinetry specimens. Thus the catalyst was exposed to a complex mixture of indoor air pollutants and maintained its performance over the duration of the experiments. Also, given the expected low cost of the catalyst and the potential to deploy it inexpensively on particle filters, a long catalyst lifetime (beyond the expected deployment time of particle filters, typically 3–6 months) may not be necessary.

Safe implementation of this technology should take into consideration other aspects not considered in this study, such as the mechanical stability of the catalyst support to prevent the catalyst particles from being entrained into the air stream, the potential occupant exposure levels associated with such processes and associated health risks. While manganese oxides are a common constituent of the Earth's crust minerals and urban dust, long-term exposure to high levels resulting from industrial operations (e.g., welding) has been associated to health effects. The California Office of Environmental Health Hazard Assessment (OEHHA) established a reference level for inhalation exposure of manganese-containing compounds of 0.2 μg m^{-3}. We performed two different tests to provide a first-order evaluation of potential exposures to airborne manganese caused by use of filters loaded with LBNL-100 catalyst. The first test involved the analysis of particulate matter collected on 0.2 μm Teflon filter that sampled air downstream of the fibrous filter loaded with LBNL-100 (face velocity through the catalyst-loaded filter was 50 cm s^{-1}). We did not detect manganese on the downstream filter. The limit of detection for Mn was 0.02 ng m^{-3}, several orders of magnitude below the OEHHA inhalation exposure levels. The other test performed was a gravimetric determination of LBNL-100 loss from the substrate after it had been used to remove formaldehyde for more than 40 days at a face velocity of 50 cm s^{-1}. The difference in filter weight before and after reaction was below the detection limit (<0.1 mg), showing insignificant loss of the catalyst. Both preliminary tests suggest that catalyst particles are not significantly entrained into the airstream that passes through the filter.

5. Conclusions

A manganese oxide catalyst was synthesized using inexpensive precursors and a simple process. Relative to commercial MnO_2, the synthesized manganese oxide has a much higher surface area and different particle size and chemical composition, consistent with superior catalytic performance. The synthesized catalyst, deposited on a typical HVAC particle filter, removed formaldehyde with a stable ~80% conversion efficiency and 100% mineralization at room temperature with air velocities close to those typical of building ventilation systems. The deployment of this catalyst on filters in the supply airstreams of HVAC systems would likely reduce substantially indoor formaldehyde concentrations.

Acknowledgements

This work was supported by the Assistant Secretary for Energy Efficiency and Renewable Energy, Building Technologies Program of the U.S. Department of Energy under Contract No. DE-AC02-05CH11231. The authors thank Jerome Lam, Colin McCormick, and Joe Hagerman of DOE for program management, M. Fischer, K. Reichl, R. Maddalena, M. Sleiman, M. Russell, T. Hotchi, M. Spears, A. Montalbano, S. Cohn, X. Song, W. Lukens and Q. Fu (LBNL) for technical assistance, J. Pena, A. Fernandez-Martinez and R. Maddalena for helpful suggestions, and L. Gundel, M. Apte and M. Sleiman for reviewing the draft report on which this paper was based.

References

[1] V.S. Prasad, M. Chaudhuri, Journal of Water Supply Research and Technology-Aqua 44 (1995) 80–82.
[2] J.E. Post, Proceedings of the National Academy of Sciences of the United States of America 96 (1999) 3447–3454.
[3] Y. Sekine, Atmospheric Environment 36 (2002) 5543–5547.
[4] Q. Xu, Y. Zhang, J. Mo, R. Ke, S. Kang. Proceedings of Indoor Air 2008. Paper ID 692, Copenhagen, Denmark, 2008.
[5] Y. Sekine, A. Nishimura, Atmospheric Environment 35 (2001) 2001–2007.
[6] X. Xie, Y. Li, Z.-Q. Liu, M. Haruta, W. Shen, Nature 458 (2009) 746–749.
[7] C. Ma, D. Wang, W. Xue, B. Dou, H. Wang, Z. Hao, Environmental Science & Technology 45 (2011) 3628–3634.
[8] X.F. Tang, Y.G. Li, X.M. Huang, Y.D. Xu, H.Q. Zhu, J.G. Wang, W.J. Shen, Applied Catalysis B – Environmental 62 (2006) 265–273.
[9] X.F. Tang, J.L. Chen, X.M. Huang, Y. Xu, W.J. Shen, Applied Catalysis B – Environmental 81 (2008) 115–121.
[10] X.F. Tang, J.H. Li, J.M. Hao, Catalysis Communications 11 (2010) 871–875.
[11] Y.R. Wen, X. Tang, J.H. Li, J.M. Hao, L.S. Wei, X.F. Tang, Catalysis Communications 10 (2009) 1157–1160.
[12] H.-G. Lintz, K. Wittstock, Applied Catalysis A: General 216 (2001) 217–225.
[13] B. Solsona, T. Garcia, S. Agouram, G.J. Hutchings, S.H. Taylor, Applied Catalysis B – Environmental 101 (2011) 388–396.
[14] T. Chen, H.Y. Dou, X.L. Li, X.F. Tang, J.H. Li, J.M. Hao, Microporous and Mesoporous Materials 122 (2009) 270–274.
[15] H. Tian, J. He, X. Zhang, L. Zhou, D. Wang, Microporous and Mesoporous Materials 138 (2011) 118–122.
[16] K.A.M. Ahmed, Q.M. Zeng, K.B. Wu, K.X. Huang, Journal of Solid State Chemistry 183 (2010) 744–751.
[17] C. Doornkamp, V. Ponec, Journal of Molecular Catalysis A – Chemical 162 (2000) 19–32.
[18] C. Cellier, V. Ruaux, C. Lahousse, P. Grange, E.M. Gaigneaux, Catalysis Today 117 (2006) 350–355.
[19] USEPA, Integrated Risk Information System (IRIS) on Formaldehyde, National Center for Environmental Assessment. Office of Research and Development, Washington, DC, 1999, http://www.epa.gov/iris/subst/0419.htm.
[20] V.J. Cogliano, Y. Grosse, R.A. Baan, K. Straif, M.B. Secretan, F. El Ghissassi, Environmental Health Perspectives 113 (2005) 1205–1208.
[21] A.T. Hodgson, D. Beal, J.E.R. McIlyaine, Indoor Air 12 (2002) 235–242.
[22] H. Destaillats, R.L. Maddalena, B.C. Singer, A.T. Hodgson, T.E. McKone, Atmospheric Environment 42 (2008) 1371–1388.
[23] H. Destaillats, M.M. Lunden, B.C. Singer, B.K. Coleman, A.T. Hodgson, C.J. Weschler, W.W. Nazaroff, Environmental Science & Technology 40 (2006) 4421–4428.
[24] B.K. Coleman, M.M. Lunden, H. Destaillats, W.W. Nazaroff, Atmospheric Environment 42 (2008) 8234–8245.
[25] USEPA, A Standardized EPA Protocol for Characterizing Indoor Air Quality in Large Office Buildings, Indoor Environment Division US EPA, Washington, DC, 2003, http://www.epa.gov/iaq/largebldgs/base/images/2003_base_protocol.pdf.
[26] A.T. Hodgson, H. Levin, Volatile Organic Compounds in Indoor Air: a Review of Concentrations Measured in North America since 1990, Lawrence Berkeley National Laboratory, Berkeley, California, 2003, p. LBNL Report 51715.
[27] T. Salthammer, S. Mentese, R. Marutzky, Chemical Reviews 110 (2010) 2536–2572.
[28] S.P. Korshunov, L.I. Vereshchagin, Russian Chemical Reviews 35 (1966) 942–957.
[29] R. Maddalena, M. Russell, D.P. Sullivan, M.G. Apte, Environmental Science & Technology 43 (2009) 5626–5632.
[30] L. Lamaita, M.A. Peluso, J.E. Sambeth, H.J. Thomas, Applied Catalysis B – Environmental 61 (2005) 114–119.
[31] J.K. Yuan, W.N. Li, S. Gomez, S.L. Suib, Journal of the American Chemical Society 127 (2005) 14184.
[32] J. Yuan, K. Laubernds, Q. Zhang, S.L. Suib, Journal of the American Chemical Society 125 (2003) 4966.
[33] D. Blish, E. Post, American Mineralogist 74 (1989) 177–186.
[34] W.K. Zwicker, W.O.J.G. Meijer, H.W. Jaffe, American Mineralogist 47 (1962) 246–266.
[35] M.A. Sidheswaran, H. Destaillats, D.P. Sullivan, W.J. Fisk. New Air Cleaning Strategies for Reduced Commercial Building Ventilation Energy. LBNL-4026E Report, Lawrence Berkeley National Laboratory, Berkeley, California, USA, http://escholarship.ucop.edu/uc/item/7s82h0zd, 2010.
[36] N. Batina, L.M. Ioffe, Y.G. Borodko, Studies in Surface Science and Catalysis 111 (1997) 655–663.
[37] H. Destaillats, W. Chen, M.G. Apte, N. Li, M. Spears, J. Almosni, G. Brunner, J. Zhang, W.J. Fisk, Atmospheric Environment 45 (2011) 3561–3568.
[38] L.M. Ioffe, P. Bosch, T. Viveros, H. Sanchez, Y.G. Borodko, Materials Chemistry and Physics 51 (1997) 269–275.